Colloids and Surfaces A 582 (2019) 123884

Contents lists available at ScienceDirect

Colloids and Surfaces A

journal homepage: www.elsevier.com/locate/colsurfa

One-pot synthesis of activated porous graphitic carbon spheres with cobalt nanoparticles

Arosha C. Dassanayake, Alexandre A.S. Gonçalves, Justin Fox[1], Mietek Jaroniec*

Department of Chemistry and Biochemistry, Kent State University, Kent, Ohio 44242, USA

GRAPHICAL ABSTRACT

ARTICLE INFO

Keywords:
Nitrogen doping
Graphitic carbon spheres
Cobalt acetate
Potassium citrate
Microporous carbons

ABSTRACT

Nitrogen doped porous graphitic carbon spheres have been extensively studied for various applications such as adsorption, catalysis, energy storage, and drug delivery due to their unique properties such as high surface area, tunable porosity, and importantly their low cost. Among many strategies available for the synthesis of graphitic carbons, catalytic graphitization is widely explored due to its industrial feasibility. Additionally, activated carbons with fine micropores are vastly studied for CO_2 capture at ambient conditions. In this case, *in-situ* activation of carbon spheres is promising because it combines both carbonization and activation in a single-step. This study is focused on the development of *in-situ* activated graphitic carbon spheres (AGCSs) by adopting a one-pot modified Stöber-like synthesis and restricting temperature treatment to a single step. Cobalt acetate and potassium citrate were added in the synthesis, where the former acted as a graphitization catalyst, while the latter acted as an activator. The resulting carbon spheres were characterized by scanning and transmission electron microscopy, nitrogen adsorption, thermogravimetry, elemental analysis, infrared spectroscopy, and X-ray diffraction. These spheres possess high volumes of ultramicropores in addition to graphitic and magnetic properties. AGCSs were able to adsorb about 5 mmol·g^{-1} of CO_2 at 0 °C and 1 bar.

1. Introduction

Graphitization and activation are considered as two economically important strategies for improving physicochemical properties of amorphous carbons. Conversion of amorphous carbons to porous graphitic carbons enables them to be used in various applications such as

* Corresponding author.
E-mail address: jaroniec@kent.edu (M. Jaroniec).
[1] Present address: Department of Chemistry, College of Wooster, Wooster, Ohio 44691, USA.

https://doi.org/10.1016/j.colsurfa.2019.123884
Received 16 April 2019; Received in revised form 28 August 2019; Accepted 28 August 2019
Available online 30 August 2019
0927-7757/

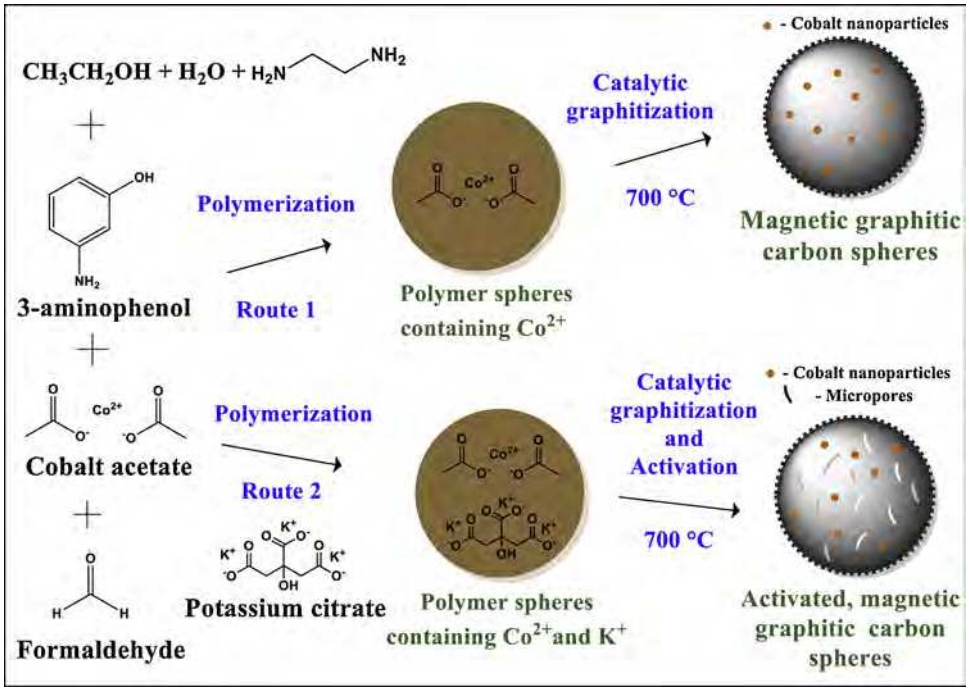

Scheme 1. Synthesis routes to obtain magnetic graphitic carbon spheres (route 1) and activated magnetic graphitic carbon spheres (route 2).

supercapacitors [1–6], catalysis [7–10], adsorption [11–15], drug delivery [16–19], and gas capture and storage [20–25]. As compared to conventional graphitization strategy, which treats carbons at temperatures about 2000 °C, the catalytic graphitization can be achieved simultaneously with carbonization at lower temperatures. Catalysts containing Fe, Ni and Co species are used in the synthesis to induce graphitization at comparatively low temperatures, 700 °C and higher [26–32]. The catalytic graphitization strategy reduces energy usage as well as enables conversion of amorphous carbons to graphitic carbons [33]. Activation of graphitic carbons under controlled conditions can be used to increase porosity and surface area of carbons. Additionally, activated carbons composed of graphitic domains exhibit higher capacitance under various electrolytes [33,34]. Recently Raymundo-Pinero and co-workers [35] illustrated that partial desolvation of ions inside micropores leads to the enhanced capacitance in carbons. Moreover, metal oxides such as MnO_2 [36], RuO_2 [37], SnO_2 [38], V_2O_5 [39], ZnO [40], Fe_3O_4 [41], and Co_3O_4 [42] in carbons contribute to pseudocapacitance *via*reversible redox reactions on the electrode surface [43]. Nonetheless, the controlled activation of metal-incorporated graphitic carbons may improve their physicochemical properties, and therefore industrial applicability.

Although potassium salts or CO_2 are commonly used for post-synthesis activation of carbons, these strategies are associated with an additional step that requires a precise control of various factors such as carbon to salt ratio, CO_2 flow, temperature and duration of activation process in order to generate meaningful microporosity without structural collapse. In contrast, *in-situ* activation strategies are gaining a significant attention because activated carbons are produced in a single step by incorporating potassium organic salts during synthesis [44,45]. Carbons obtained by *in-situ* activation feature a large fraction of ultramicropores (pores bellow 0.7 nm), which are highly beneficial for applications such as CO_2 capture at ambient conditions.

Recently, various modifications of the Stöber-like synthesis have been explored to obtain carbon spheres with desired properties [46]. This synthesis is well suited for controlled addition of multiple chemical species during the formation of phenolic resin spheres. Regardless of various independent studies conducted to produce both graphitic and activated nitrogen doped carbons, the efforts to introduce graphitic domains, ultramicropores, and nitrogen species into carbon spheres during one-pot synthesis are still seldom. In this study, we explore the possibility of producing nitrogen doped activated graphitic carbon spheres in a single carbonization/activation step following the modified Stöber-like synthesis strategy. Cobalt acetate and potassium citrate were directly added to the synthesis mixture, where cobalt salt acted as a graphitization catalyst and a source for forming magnetic cobalt nanoparticles (desired for easy separation in potential liquid phase applications), while potassium salt acted as an *in-situ* activator. The resulting magnetic graphitic carbon spheres with high volume of micropores were tested for CO_2 capture at ambient conditions.

2. Experimental

2.1. Materials

Resorcinol (98%), pyrrole (99%), and ethylenediamine (99%) were obtained from Acros Organics. 3-aminophenol was purchased from Alfa Aesar. Formaldehyde (37 wt%), cobalt acetate tetrahydrate (98%), and potassium citrate monohydrate (99%) were purchased from Fisher Scientific. Deionized water was obtained from an in-house Ion Pure Plus 150 Service Deionization Ion-exchange purification system and Aqua One. All reagents were of analytical grade and were used without further purification.

2.2. Potassium citrate and cobalt acetate assisted syntheses of phenolic resin spheres

Cobalt acetate and potassium citrate were incorporated to two series of polymer spheres (PS) using a modified one-pot hydrothermal synthesis (see Scheme 1) [47]. To synthesize the first series of graphitic carbon spheres, 0.1 ml of ethylenediamine was added to an aqueous alcoholic solution, which was prepared by mixing 8 ml of ethanol with 20 ml of deionized water. Thereafter, 0.2 g of 3-aminophenol was added to the solution. Cobalt acetate was added in varying amounts (0.1 mmol, 0.3 mmol, 0.4 mmol, 0.6 mmol, 0.9 mmol) to the above mixture and stirred for ca. 30 min to complete its dissolution. Finally, 0.28 ml of formaldehyde was added and stirred for 24 h at room

temperature. The obtained colloidal solution was transferred into a 125 ml Teflon container placed in a metal sealed autoclave and then subjected to thermal treatment at 100 °C for 24 h.

The second series of activated graphitic carbon spheres was synthesized as described above but fixing the mass of cobalt acetate at 0.3 mmol level. Following addition of cobalt acetate, potassium citrate in varying amounts (0.00050 mol, 0.00075 mol, 0.00100 mol) was added to the solution. Finally, formaldehyde was added to initiate polymerization. After stirring for 24 h, the obtained colloidal solution was subjected to a similar thermal treatment as described above.

2.3. Carbonization and activation of polymer spheres

Graphitic carbon (GC), graphitic carbon spheres (GCSs) and activated graphitic carbon spheres (AGCSs) were obtained by a single-step carbonization and activation of the phenolic resin spheres. The materials were placed into a tube furnace and thermally treated under flowing N_2 in two steps. First at 350 °C for 2 h, then at 700 °C for another 2 h; a heating rate of 1 °C·min^{-1} was used in both steps. The AGCS materials were washed in deionized water to remove the excess of salt, then separated from solution by centrifugation and dried in an oven at 100°C for 2 h. The resulting carbon spheres were labeled as GC-CoX, GCS-CoX and AGCS-CoX-KY, where "K" refers to potassium citrate, "X" refers to the sample number of graphitic carbon series and "Y" refers to the molar amount of potassium citrate rounded to the nearest whole number, respectively. For instance, in the case of AGCS-Co2-K75, "AGCS" refers to activated graphitic carbon spheres, "Co" refers to cobalt, "2" refers to 2nd sample of graphitic carbon synthesized with cobalt acetate (0.3 mmol), "K" refers to potassium citrate and "75" refers to 0.00075 mol of potassium citrate.

2.4. Characterization

Nitrogen adsorption was measured for each sample at −196 °C using an ASAP 2020 volumetric analyzer (Micromeritics, Inc.). CO_2 adsorption measurements were carried out at 0 and 25 °C up to 1.2 atm on an ASAP 2020 volumetric adsorption analyzer (Micromeritics, Inc., GA). Thermogravimetric (TG) profiles were recorded using a high resolution thermogravimetric TGA Q-500 analyzer (TA Instruments, Inc.). Scanning electron microscopy (SEM) images were obtained using a Hitachi S-2600 N scanning electron microscope. Transmission electron microscopy (TEM) images were obtained on a FEI Tecnai G2 F20 microscope. The FTIR spectra were obtained on a Bruker Vector 33 with resolution of 4 cm^{-1}, and 32 scans. Elemental analysis of carbon, nitrogen, and hydrogen was obtained using a LECO TruSpec Micro elemental analyzer.

3. Results and discussion

Fig. 1 shows the X-ray diffraction patterns for the synthesized materials and provides evidence of the presence of graphitic domains and metallic cobalt in the carbon nanoparticles. The peak around 26° (2θ) may indicate the presence of graphitic domains, while metallic cobalt is evidenced by the peaks at 44°, 52° and 76° (2θ). These diffraction peaks correspond to the (111), (200) and (220) planes, respectively[48], of the FCC structure of metallic cobalt [ICDD 01-071-4651]. It is evident that with increasing cobalt content the intensity of the peaks around 26°, 44°, and 52° (2θ) increases. This signifies the role of cobalt in catalytic graphitization of the carbon matrix. Up to date, different cobalt salts have been used to produce graphitic magnetic thin films [49], graphitic carbon nanotubes [50], 2D graphene [51], and graphitic spheres [52]. For instance, Liu and coworkers were able to incorporate cobalt nanoparticles into mesoporous carbons [52].

Chen and coworkers utilized TPR experiments to study the behavior of metallic cobalt formation from incorporated cobalt salts within carbon framework [53]. According to their studies, $Co(NO_3)_2$ within carbon nanotube framework is reduced to Co *via*two steps. First, the formation of Co_3O_4 and Co_2O_3 occurs, which is followed by formation of CoO (step 1), and further by reduction to Co (step 2). In a similar study Xiong and coworkers [54] monitored the conversion of Co_3O_4 and CoO using $Co(NO_3)_2$ incorporated into nanotubes and carbon spheres. The reduction of Co_3O_4 to CoO was observed at 280°C, while CoO to Co was observed at 363°C. Therefore, it is expected that only metallic cobalt will be present in all samples herein synthesized. To further confirm this hypothesis FTIR experiment was performed for GC-Co4 and GCS-Co2, and data are shown in Fig. S1 in supporting information. The absence of significant absorption bands on the FTIR spectra (4000–400 cm^{-1}) indicates a very low concentration of hydrogen in the material, which is characteristic for graphite [55]. Therefore, the change in the FTIR profile upon Co-addition indicates that Co is catalyzing the graphitization of amorphous matrix. Moreover, the presence of absorption bands for carbon spheres indicates the presence of C=C bond of aromatic group, and CC− (sp^2-sp^3) vibration modes of an amorphous matrix [55]. The FTIR spectra for GC-Co4 and GCS-Co2 show no absorption bands for neither cobalt oxides nor cobalt carbide. Nonetheless, FTIR results complements the XRD results, and show that pure metallic cobalt nanoparticles are only present in the synthesized materials.

Activated graphitic carbon spheres (AGCSs) were synthesized by incorporating different amounts of potassium citrate into the synthesis mixture with a fixed amount of cobalt acetate (0.3 mmol; AGCS-Co2-KY samples). The resulting carbons obtained for cobalt acetate amount larger than 0.3 mmol deviated from spherical morphology. A comparison of the XRD patterns obtained for the GCS-2, AGCS-Co2-K75, and AGCS-Co2-K50 − HCl-w samples is shown in Fig. 1b.

Thermogravimetric analysis (TGA) was performed for the samples

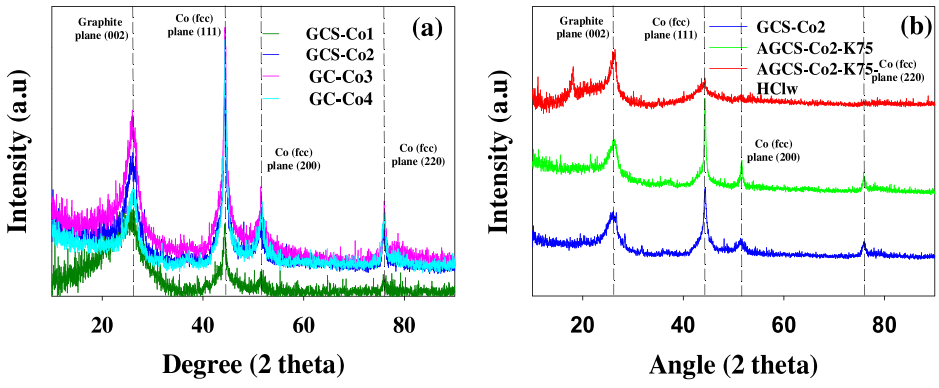

Fig. 1. (a) XRD patterns of the graphitic carbons studied, (b) and before and after cobalt dissolution.

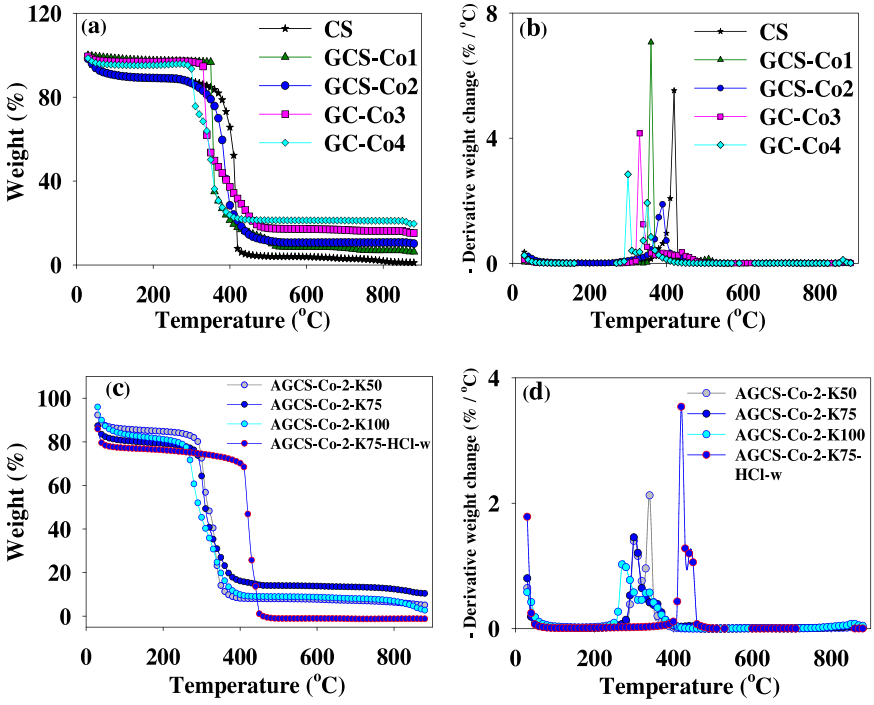

Fig. 2. (a,c) Thermogravimetric analysis, (b,d) and respective differential thermogravimetric profiles for the samples studied.

under air atmosphere. It was observed that with increasing cobalt mass in the synthesis mixture, the decomposition temperature of carbon was gradually reduced. The catalytic decomposition of carbons in the presence of Co species is reported elsewhere [56,57]. Herein we propose a similar explanation for metallic cobalt-assisted decomposition of the carbon framework. In the presence of oxygen there is the possibility of conversion of the metallic cobalt nanoparticles back to respective oxides such as Co_3O_4, which in turn can be reduced by the carbon, thus this process can probably initiate the catalytic decomposition of the carbon framework. Fig. 2(a,b), shows that this behavior is pronounced for the samples with higher cobalt content. Regardless of having a comparatively high cobalt mass, GCS-Co2 showed a slightly higher thermal stability (up to 393 ºC) as compared to that of GCS-Co1, which started to decompose around 360 °C. This deviation from the expected trend can be attributed to the lower cobalt content present in the aforementioned samples as compared to that of GC-Co3 and GC-Co4; in the former, the carbon oxidation was predominant. Thus, for GC-Co3 and GC-Co4, the catalytic decomposition was attenuated during thermogravimetric measurements under oxygen.

Thermal stability of activated samples (AGCS-Co-2-K series) was also evaluated by heating in air, which is shown in Fig. 2(c and d). Similarly, the activated samples exhibited lower thermal stabilities as indicated by decomposition events in Table 1. Contribution from metallic cobalt toward the catalytic decomposition was further studied using the GCS-Co2-K75 – HCl-w sample, in which cobalt was dissolved by hydrochloric acid treatment. Removal of cobalt from AGCS-Co3-K75 – HCl-w was confirmed by analyzing the residual mass of the sample, which was near 0 wt%. As expected, this carbon sample exhibited high thermal stability up to 446 ºC. Note that non-graphitized "CS" showed comparatively lower thermal stability (up to 421 ºC), probably due to the absence of graphitic domains. The residual mass percentages, ascribed to cobalt oxides (5–35 wt%), are shown in Table 1. Overall all the samples exhibited thermal stability in air beyond 270 °C. Thermal decomposition and respective differential weight profiles for the carbons that were synthesized using higher cobalt acetate amounts; 0.6 mmol (GC-Co4) and 0.9 mmol (GC-Co5) are shown in Fig. S2 in supporting information.

Table 1
Decomposition temperatures for the samples studied.

Sample	Decomposition temperature (°C)	Metal oxide (wt%)
GCS-Co1	360	6.28
GCS-Co2	393	10.18
GC-Co3	330	15.22
AGCS-Co2-K50	270	5.09
AGCS-Co2-K75	300	10.44
AGCS-Co2-K100	340	2.74

As can be seen from Fig. 3c, SEM studies revealed that the samples synthesized using cobalt acetate amounts higher than 0.4 mmol lost their spherical morphology. We suggest that higher cobalt acetate mass in the synthesis disturbs the polymerization between 3-aminophenol and formaldehyde, leading to a non-spherical morphology. SEM images of the samples synthesized with higher cobalt amounts are shown in Fig. S3 of supporting information. Addition of varying amounts of potassium citrate to the synthesis was done at the fixed mass of cobalt acetate, 0.3 mmol. Note that potassium citrate-assisted activation was able to preserve the spherical morphology of the carbons studied (Fig. 3d–f). However, the CS-Co2-K100 sample (see Fig. 3f) underwent partial structural collapse due to the excessive activation (Fig. 3f).

TEM studies reveal that cobalt nanoparticles are well-dispersed in the carbon spheres (Fig. 4a, b and d). Furthermore, graphitic domains are found to be scattered around cobalt nanoparticles (see Fig. S4 in supporting information). Both GCS-Co1 and GCS-Co2 samples possess graphitic domains, however the degree of graphitization is much higher in later sample, whereas GCS-Co1 sample is composed of mainly amorphous carbon domains (as indicated by TGA analysis). The TEM image of the GC-Co3 sample further confirms the effect of higher cobalt mass toward polymerization of carbon precursors, where amorphous carbon and cobalt seem to aggregate independently. Moreover, the activation leads to the creation of additional pores within the carbon framework and causes removal of some cobalt from the spheres (see Fig. 4d). The average size of carbon spheres studied was found to be around 450 nm, while the size distribution of dispersed cobalt nanoparticles was estimated between 20–30 nm. The presence of these cobalt nanoparticles introduces magnetism to the carbons and as a result,

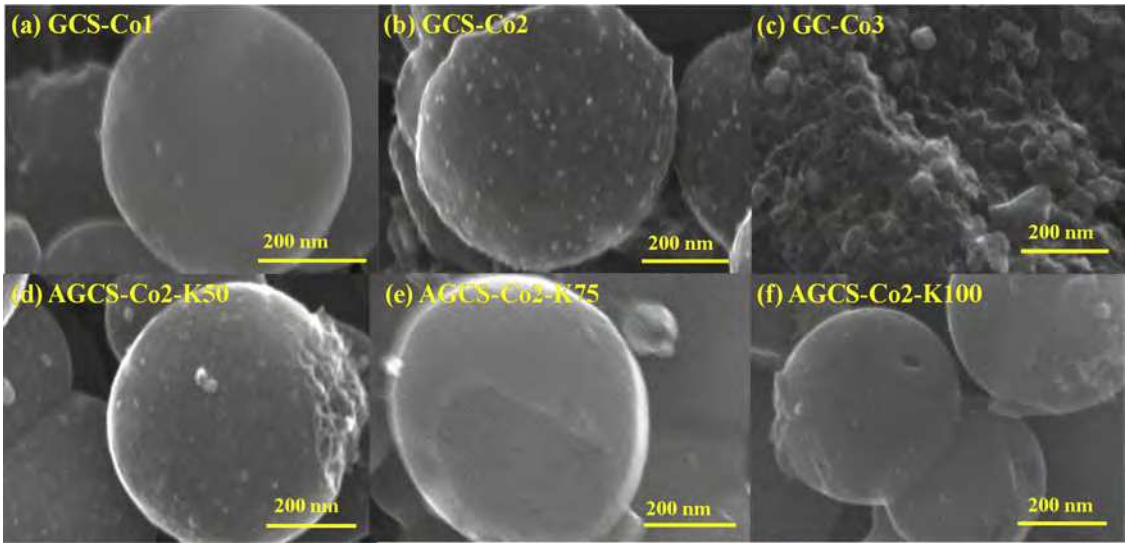

Fig. 3. Scanning electron microscope (SEM) images of the samples studied.

they could be easily separated from a solution under the force of an external magnetic field (see Fig. S5 in supporting information).

Nitrogen adsorption measurements were performed for carbons studied at −196 °C to evaluate the specific surface area, pore volume and pore size distribution (see Table 2, and Fig. 5). All isotherms possess hysteresis loops at high relative pressures, which indicate the presence of mesopores. The source of these mesopores can be pores generated during graphitization, and (or) inter particle voids. The pore size distributions for each sample are shown in Fig. 5b and d. Fig. 5b shows that the graphitic carbons exhibit bimodal distributions of micropores (pores below 2 nm); one below 1 nm, while the second is between 1–2 nm. However, the average volumes of these micropores are as low as 0.05 $cm^3 g^{-1}$. Additionally, a broad distribution of peaks is observed between 2–8 nm, which corresponds to mesopores, which have a significant contribution to the porosity of all graphitic carbons studied.

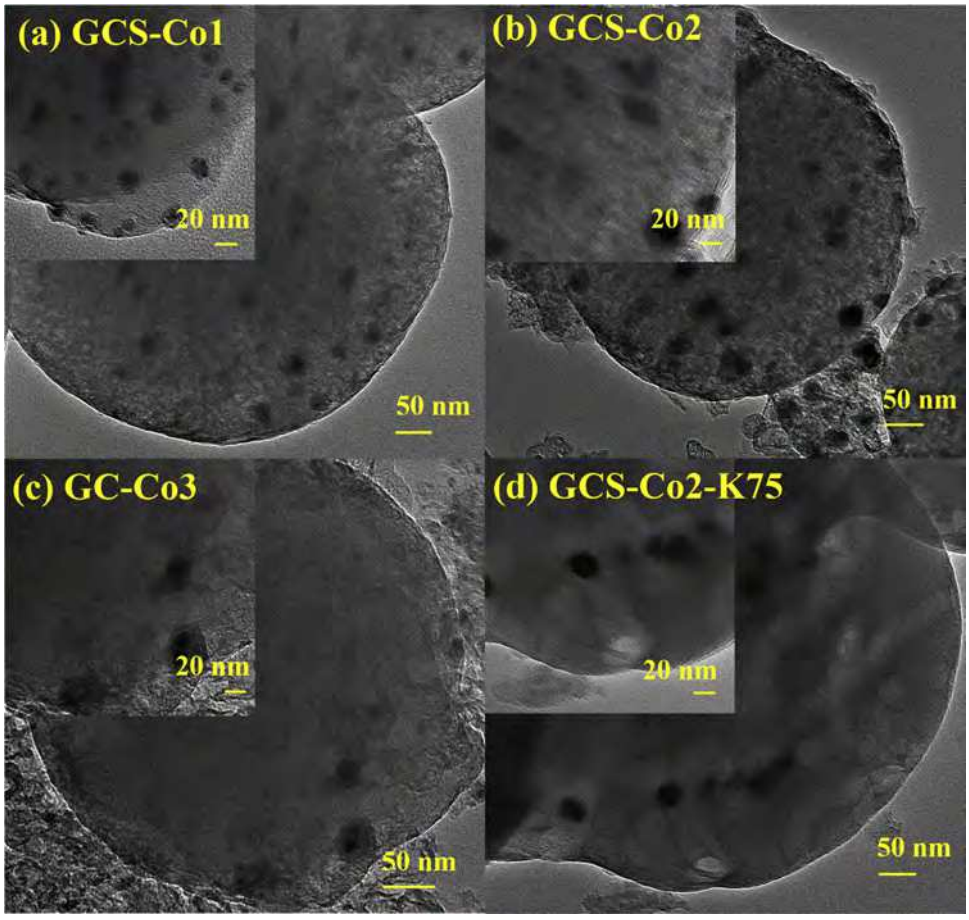

Fig. 4. Transmission electron microscopy (TEM) images of the samples studied.

Table 2
BET surface areas and pore volumes of the samples studied.

Sample	S_{BET} ($m^2 \cdot g^{-1}$)	Micropore volume (< 1 nm) ($cm^3 \cdot g^{-1}$)	Total pore volume ($cm^3 \cdot g^{-1}$)	C%	N%
GCS-Co1	283	0.04	0.20	72.8	5.7
GCS-Co2	279	0.05	0.24	65.6	5.2
GC-Co3	236	0.03	0.19	54.7	1.2
AGCS-Co2-K50	573	0.18	0.36	69.7	5.0
AGCS-Co2-K75	828	0.29	0.46	56.1	4.9
AGCS-Co2-K100	472	0.18	0.26	60.3	3.6

S_{BET} - BET surface area.

The adsorption isotherms and respective pore size distributions obtained for activated carbons are shown in Fig. 5 c and d. As expected, the activation led to a significant increase of micropore volumes, and the BET surface areas, where the AGCS-Co2-K75 sample possesses the highest surface area ($828\ m^2\ g^{-1}$), and micropore volume ($0.29\ cm^3\ g^{-1}$) among the activated samples. The use of potassium citrate above 0.00075 mol in the synthesis, along with 0.3 mmol of cobalt acetate, led to the structural collapse during the catalytic graphitization/activation process as observed for the AGCS-Co2-K100 sample. Because of activation, microporosity becomes dominant in the pore size distribution curves (see Fig. 5d). Activation generated a considerable fraction of ultramicropores, which is highly favorable for CO_2 capture at ambient conditions. Previous studies show the potential of generating ultramicropores in carbons by incorporating different potassium organic salts during the Stöber-like synthesis [44,45]. Considering the high surface area of these graphitic carbons, they would serve as promising materials not only in gas capture but also in fields such as energy storage, catalysis, sensors, thermoelectric and sea water desalination [58]. Doping of N and Co into graphene has been found to efficiently tune its electronic structure and thus enhance the catalytic activity of the resulting composite material. For instance, in N doped carbon materials electronegative N atoms accept electrons and activate the neighboring C atoms, converting them into catalytic sites. Several studies have reported the potential of N-doped graphene and Co incorporated N doped graphene to act as metal-free catalysts for ORR in H_2O_2 fuel cells [59–61].

However, preservation of a small volume of mesopores is still evident as indicated by the desorption hysteresis in all isotherms (Fig. 5c). Note that depending on the intended application, the volume of these mesopores could be further increased by removal of embedded cobalt nanoparticles *via*acid treatment. Some mesoporous carbons with graphitic domains have been tested for various applications such as supercapacitors [62,63], oxygen reduction [64], fuel cells [65], photocatalysts [66], dye adsorption [13], heavy metal removal [67] and drug delivery [68]. The evaluated BET surface areas, micropore volumes, total pore volumes, carbon and nitrogen percentages of all samples are shown in Table 2, while N_2 adsorption isotherms and respective pore size distributions for the GC-Co4 (cobalt acetate 0.6 mmol) and GC-Co5 (cobalt acetate 0.9 mmol) samples are shown in Fig. S6 of supporting information. Average nitrogen content in the samples varies between 1.2–5.7 wt%. Ethylenediamine and 3-aminophenol could be possible sources of this nitrogen. It is noteworthy that doped nitrogen atoms in graphitic carbons have been found to contribute toward pseudocapacitance, when such carbons are used as supercapacitors [69,70].

All activated carbon samples exhibited relatively good CO_2 uptake at ambient conditions. Individual CO_2 adsorption isotherms and respective uptake values at 1 bar are shown in Fig. 6 and Table 3. The CO_2 uptakes at 1 bar were in the range of 3.2–5.0 $mmol \cdot g^{-1}$ (0 °C), and 2.3–3.6 $mmol \cdot g^{-1}$ (25 °C). The main reason for these carbons to exhibit relatively low CO_2 adsorption capacities is probably due to insufficient volume of carbon framework available for activation by potassium citrate, since majority of the carbon volume was occupied by cobalt nanoparticles and graphitic domains. Note that graphitic domains have no

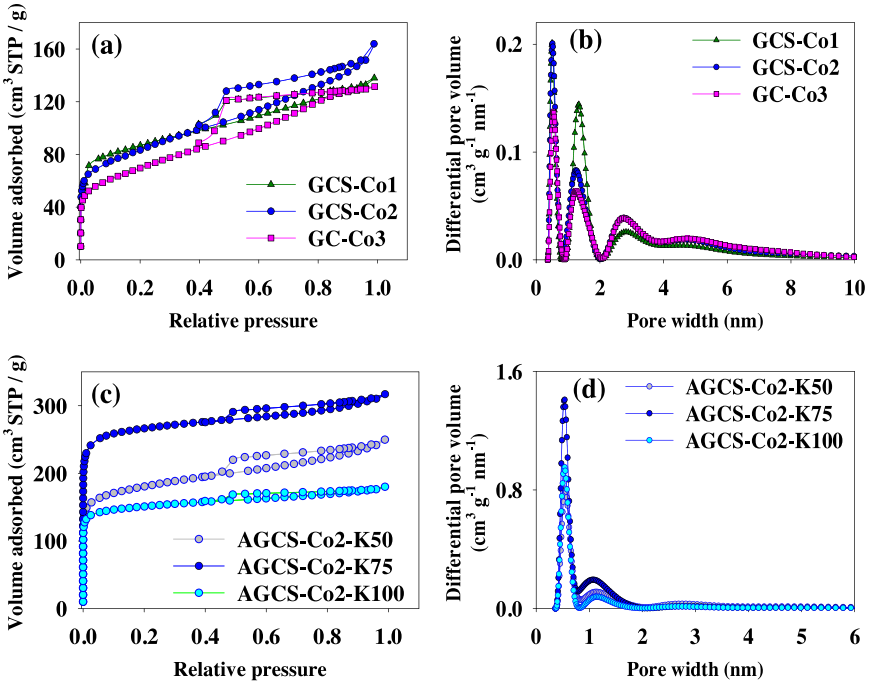

Fig. 5. N_2 adsorption isotherms (left panels) and corresponding pore size distribution curves (PSD) (right panels).

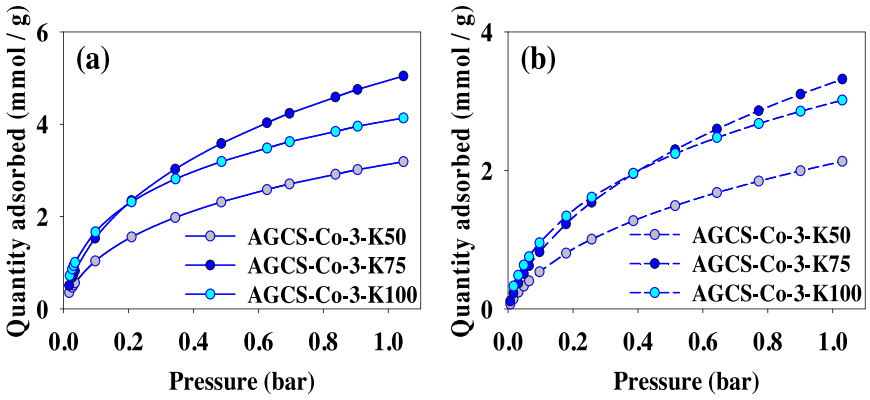

Fig. 6. CO_2 adsorption isotherms obtained for the activated samples at (a) 0 °C, and (b) 25 °C.

Table 3
CO_2 uptake for the activated carbon samples at 0 °C and 25 °C.

Sample	S_{BET} ($m^2 \cdot g^{-1}$)	$PV_{0.7}$ nm ($cm^3 \cdot g^{-1}$)	CO_2 uptake ($mmol \cdot g^{-1}$)	
			0 °C	25 °C
AGCS-Co2-K50	573	0.15	3.19	2.33
AGCS-Co2-K75	828	0.24	5.04	3.63
AGCS-Co2-K100	472	0.17	4.13	3.25

S_{BET} - BET surface area, $PV_{0.7nm}$ - Volume of micropores having diameters below 0.7 nm.

significant contribution towards CO_2 adsorption. As expected, the uptake capacities are proportional to the ultramicropore volumes in each sample. Further studies can be conducted to improve the CO_2 capture capacities of these carbons by optimizing activation conditions and controlling the degree of graphitization.

4. Conclusions

Nitrogen doped porous graphitic carbon spheres possessing magnetic properties were successfully synthesized by adopting a modified Stöber-like method, followed by catalytic graphitization. The latter was achieved by incorporating cobalt acetate, while *in-situ* activation was carried out by incorporating potassium citrate. The desired graphitized and activated carbons were obtained in a single temperature treatment assisted by cobalt and potassium species. The resulting carbons were characterized using various techniques and tested for CO_2 capture. The materials showed adequate CO_2 capture capacities. Considering the broad applicability of N and Co doped graphene analogues in energy storage, catalysis and sensors, this study shows new prospects to obtain scalable porous graphitic carbon spheres with tunable physicochemical properties. Even though synthetic graphene is highly attractive material in various fields, its commercial synthesis often suffer from layer aggregation, which in turn nullify the benefits associated with layered geometry. In contrast, graphitic carbon spheres produced in this study are composed of graphitic domains distributed in close proximity within the carbon structure along with a platform to optimize the specific surface area. Therefore, these materials can serve as a plausible low-cost alternative for synthetic graphene materials.

Declaration of Competing Interest

The authors declare that they have no known competing financial interests or personal relationships that could have appeared to influence the work reported in this paper.

Acknowledgments

The authors thank the National Science Foundation for support of this research under CHE-1659571 (REU). The SEM data were obtained at the Hitachi 2600-N SEM facility and TEM data were obtained using FEI Tecnai G2 F20 microscope at the Advanced Materials and Liquid Crystal Institute Kent State University, supported by the Ohio Research Scholars Program Research Cluster on Surfaces in Advanced Materials. The authors thank Dr. Min Gao for technical support in SEM and TEM imaging and Dr. Mahinda Gangoda for assistance in elemental analysis of the samples.

Appendix A. Supplementary data

Supplementary material related to this article can be found, in the online version, at doi:https://doi.org/10.1016/j.colsurfa.2019.123884.

References

[1] N.P. Wickramaratne, V.S. Perera, B.W. Park, M. Gao, G.W. McGimpsey, S.D. Huang, M. Jaroniec, Graphitic mesoporous carbons with embedded prussian blue-derived iron oxide nanoparticles synthesized by soft templating and low-temperature graphitization, Chem. Mater. 25 (14) (2013) 2803–2811.
[2] D.W. Wang, F. Li, M. Liu, G.Q. Lu, H.-M. Cheng, 3D aperiodic hierarchical porous graphitic carbon material for high-rate electrochemical capacitive energy storage, Angew. Chem. Int. Ed. 47 (2) (2008) 373–376.
[3] Y. Zhu, S. Murali, M.D. Stoller, K. Ganesh, W. Cai, P.J. Ferreira, A. Pirkle, R.M. Wallace, K.A. Cychosz, M. Thommes, Carbon-based supercapacitors produced by activation of graphene, Science 332 (6037) (2011) 1537–1541.
[4] L. Sun, C. Tian, Y. Fu, Y. Yang, J. Yin, L. Wang, H. Fu, Nitrogen-doped porous graphitic carbon as an excellent electrode material for advanced supercapacitors, Eur. J. Chem. 20 (2) (2014) 564–574.
[5] F. Ma, H. Zhao, L. Sun, Q. Li, L. Huo, T. Xia, S. Gao, G. Pang, Z. Shi, S. Feng, A facile route for nitrogen-doped hollow graphitic carbon spheres with superior performance in supercapacitors, J. Mater. Chem. 22 (27) (2012) 13464–13468.
[6] Y. Tan, C. Xu, G. Chen, Z. Liu, M. Ma, Q. Xie, N. Zheng, S. Yao, Synthesis of ultrathin nitrogen-doped graphitic carbon nanocages as advanced electrode materials for supercapacitor, ACS Appl. Mater. Interfaces 5 (6) (2013) 2241–2248.
[7] S. Yang, Y. Gong, J. Zhang, L. Zhan, L. Ma, Z. Fang, R. Vajtai, X. Wang, P.M. Ajayan, Exfoliated graphitic carbon nitride nanosheets as efficient catalysts for hydrogen evolution under visible light, Angew. Chem. Int. Ed. 25 (17) (2013) 2452–2456.
[8] Y. Wang, X. Wang, M. Antonietti, Polymeric graphitic carbon nitride as a heterogeneous organocatalyst: from photochemistry to multipurpose catalysis to sustainable chemistry, Angew. Chem. Int. Ed. 51 (1) (2012) 68–89.
[9] E.S. Steigerwalt, G.A. Deluga, D.E. Cliffel, C. Lukehart, A Pt-Ru/graphitic carbon nanofiber nanocomposite exhibiting high relative performance as a direct-methanol fuel cell anode catalyst, J. Phys. Chem. B 105 (34) (2001) 8097–8101.
[10] G. Ertl, H. Knözinger, J. Weitkamp, Handbook of Heterogeneous Catalysis, (1997).
[11] P. Bradder, S.K. Ling, S. Wang, S. Liu, Dye adsorption on layered graphite oxide, J. Chem. Eng. Data 56 (1) (2010) 138–141.
[12] Y. Li, Q. Du, T. Liu, X. Peng, J. Wang, J. Sun, Y. Wang, S. Wu, Z. Wang, Y. Xia, Comparative study of methylene blue dye adsorption onto activated carbon, graphene oxide, and carbon nanotubes, Chem. Eng. Res. Des. 91 (2) (2013) 361–368.
[13] Y. Wang, M. Yao, Y. Chen, Y. Zuo, X. Zhang, L. Cui, General synthesis of magnetic mesoporous FeNi/graphitic carbon nanocomposites and their application for dye adsorption, J. Alloys Compounds 627 (2015) 7–12.
[14] N. Nesterenko, F. Thibault-Starzyk, V. Montouilliout, V. Yushchenko, C. Fernandez, J.P. Gilson, F. Fajula, I. Ivanova, The use of the consecutive adsorption of pyridine

bases and carbon monoxide in the IR spectroscopic study of the accessibility of acid sites in microporous/mesoporous materials, React. Kinet. Catal. Lett. 47 (1) (2006) 40–48.
[15] L.C. Oliveira, R.V. Rios, J.D. Fabris, V. Garg, K. Sapag, R.M. Lago, Activated carbon/iron oxide magnetic composites for the adsorption of contaminants in water, Carbon 40 (12) (2002) 2177–2183.
[16] X. Sun, Z. Liu, K. Welsher, J.T. Robinson, A. Goodwin, S. Zaric, H. Dai, Nano-graphene oxide for cellular imaging and drug delivery, Nano Res. 1 (3) (2008) 203–212.
[17] S.P. Sherlock, H. Dai, Multifunctional FeCo-graphitic carbon nanocrystals for combined imaging, drug delivery and tumor-specific photothermal therapy in mice, Nano Res. 4 (12) (2011) 1248–1260.
[18] S.P. Sherlock, S.M. Tabakman, L. Xie, H. Dai, Photothermally enhanced drug delivery by ultrasmall multifunctional FeCo/graphitic shell nanocrystals, ACS Nano 5 (2) (2011) 1505–1512.
[19] Z. Liu, J.T. Robinson, X. Sun, H. Dai, PEGylated nanographene oxide for delivery of water-insoluble cancer drugs, J. Am. Chem. Soc. 130 (33) (2008) 10876–10877.
[20] F. Schedin, A. Geim, S. Morozov, E. Hill, P. Blake, M. Katsnelson, K. Novoselov, Detection of individual gas molecules adsorbed on graphene, Nat. Mater. 6 (9) (2007) 652–655.
[21] J. Dai, J. Yuan, P. Giannozzi, Gas adsorption on graphene doped with B, N, Al, and S: a theoretical study, Appl. Phys. Lett. 95 (23) (2009) 232105.
[22] K.C. Kemp, H. Seema, M. Saleh, N.H. Le, K. Mahesh, V. Chandra, K.S. Kim, Environmental applications using graphene composites: water remediation and gas adsorption, Nanoscale 5 (8) (2013) 3149–3171.
[23] H.J. Yoon, J.H. Yang, Z. Zhou, S.S. Yang, M.M.C. Cheng, Carbon dioxide gas sensor using a graphene sheet, Sens. Actuators B-Chem. 157 (1) (2011) 310–313.
[24] G. Srinivas, J. Burress, T. Yildirim, Graphene oxide derived carbons (GODCs): synthesis and gas adsorption properties, Energy Environ. Sci. 5 (4) (2012) 6453–6459.
[25] Z. Wen, Q. Qu, Q. Gao, X. Zheng, Z. Hu, Y. Wu, Y. Liu, X. Wang, An activated carbon with high capacitance from carbonization of a resorcinol–formaldehyde resin, Electrochem. Commun. 11 (3) (2009) 715–718.
[26] A. Ōya, S. Ōtani, Catalytic graphitization of carbons by various metals, Carbon 17 (2) (1979) 131–137.
[27] A. Ōya, H. Marsh, Phenomena of catalytic graphitization, J. Mater. Sci. 17 (2) (1982) 309–322.
[28] M. Sevilla, A.B. Fuertes, Catalytic graphitization of templated mesoporous carbons, Carbon 44 (3) (2006) 468–474.
[29] F. Maldonado-Hódar, C. Moreno-Castilla, J. Rivera-Utrilla, Y. Hanzawa, Y. Yamada, Catalytic graphitization of carbon aerogels by transition metals, Langmuir 16 (9) (2000) 4367–4373.
[30] S.S. Tzeng, Catalytic graphitization of electroless Ni–P coated PAN-based carbon fibers, Carbon 44 (10) (2006) 1986–1993.
[31] M. Schwickardi, T. Johann, W. Schmidt, F. Schüth, High-surface-area oxides obtained by an activated carbon route, Chem. Mater. 14 (9) (2002) 3913–3919.
[32] D. Gu, W. Li, F. Wang, H. Bongard, B. Spliethoff, W. Schmidt, C. Weidenthaler, Y. Xia, D. Zhao, F. Schüth, Controllable synthesis of mesoporous peapod-like Co_3O_4@ carbon nanotube arrays for high-performance lithium-ion batteries, Angew. Chem. Int. Ed. 54 (24) (2015) 7060–7064.
[33] D. Zhai, H. Du, B. Li, Y. Zhu, F. Kang, Porous graphitic carbons prepared by combining chemical activation with catalytic graphitization, Carbon 49 (2) (2011) 725–729.
[34] G. Yang, H. Han, T. Li, C. Du, Synthesis of nitrogen-doped porous graphitic carbons using nano-$CaCO_3$ as template, graphitization catalyst, and activating agent, Carbon 50 (10) (2012) 3753–3765.
[35] E. Raymundo-Pinero, K. Kierzek, J. Machnikowski, F. Béguin, Relationship between the nanoporous texture of activated carbons and their capacitance properties in different electrolytes, Carbon 44 (12) (2006) 2498–2507.
[36] S. Chen, J. Zhu, X. Wu, Q. Han, X. Wang, Graphene oxide-MnO_2 nanocomposites for supercapacitors, ACS Nano 4 (5) (2010) 2822–2830.
[37] T. Liu, W. Pell, B. Conway, Self-discharge and potential recovery phenomena at thermally and electrochemically prepared RuO_2 supercapacitor electrodes, Electrochim. Acta 42 (23–24) (1997) 3541–3552.
[38] F. Li, J. Song, H. Yang, S. Gan, Q. Zhang, D. Han, A. Ivaska, L. Niu, One-step synthesis of graphene/SnO_2 nanocomposites and its application in electrochemical supercapacitors, Nanotechnology 20 (45) (2009) 455602.
[39] Z. Chen, V. Augustyn, J. Wen, Y. Zhang, M. Shen, B. Dunn, Y. Lu, High-performance supercapacitors based on intertwined CNT/V_2O_5 nanowire nanocomposites, Adv. Mater. 23 (6) (2011) 791–795.
[40] Y. Zhang, H. Li, L. Pan, T. Lu, Z. Sun, Capacitive behavior of graphene–ZnO composite film for supercapacitors, J. Electroanal. Chem. 634 (1) (2009) 68–71.
[41] X. Du, C. Wang, M. Chen, Y. Jiao, J. Wang, Electrochemical performances of nanoparticle Fe_3O_4/activated carbon supercapacitor using KOH electrolyte solution, J. Phys. Chem C. 113 (6) (2009) 2643–2646.
[42] J. Xu, L. Gao, J. Cao, W. Wang, Z. Chen, Preparation and electrochemical capacitance of cobalt oxide (Co_3O_4) nanotubes as supercapacitor material, Electrochim. Acta 56 (2) (2010) 732–736.
[43] T. Chen, L. Dai, Carbon nanomaterials for high-performance supercapacitors, Appl. Mater. Today 16 (7) (2013) 272–280.
[44] A.C. Dassanayake, M. Jaroniec, Dual optimization of microporosity in carbon spheres for CO_2 adsorption by using pyrrole as the carbon precursor and potassium salt as the activator, J. Mater. Chem. A 5 (36) (2017) 19456–19466.
[45] J. Ludwinowicz, M. Jaroniec, Potassium salt-assisted synthesis of highly microporous carbon spheres for CO_2 adsorption, Carbon 82 (2015) 297–303.
[46] J. Choma, D. Jamioła, K. Augustynek, M. Marszewski, M. Gao, M. Jaroniec, New opportunities in Stöber synthesis: preparation of microporous and mesoporous carbon spheres, J. Mater. Chem. 22 (25) (2012) 12636–12642.
[47] J. Liu, S.Z. Qiao, H. Liu, J. Chen, A. Orpe, D. Zhao, G.Q.M. Lu, Extension of the Stöber Method to the preparation of monodisperse resorcinol-formaldehyde resin polymer and carbon spheres, Angew. Chem. Int. Ed. 50 (26) (2011) 5947–5951.
[48] Ø. Borg, P.D. Dietzel, A.I. Spjelkavik, E.Z. Tveten, J.C. Walmsley, S. Diplas, S. Eri, A. Holmen, E. Rytter, Fischer-Tropsch synthesis: cobalt particle size and support effects on intrinsic activity and product distribution, J. Catal. 259 (2) (2008) 161–164.
[49] T. Hayashi, S. Hirono, M. Tomita, S. Umemura, Magnetic thin films of cobalt nanocrystals encapsulated in graphite-like carbon, Nature 381 (6585) (1996) 772.
[50] S. Iijima, T. Ichihashi, Single-shell carbon nanotubes of 1-nm diameter, Nature 363 (6430) (1993) 603.
[51] Y. Saito, T. Yoshikawa, M. Okuda, N. Fujimoto, S. Yamamuro, K. Wakoh, K. Sumiyama, K. Suzuki, A. Kasuya, Y. Nishina, Cobalt particles wrapped in graphitic carbon prepared by an arc discharge method, J. Appl. Phys. 75 (1) (1994) 134–137.
[52] H.J. Liu, S.H. Bo, W.J. Cui, F. Li, C.X. Wang, Y.Y. Xia, Nano-sized cobalt oxide/mesoporous carbon sphere composites as negative electrode material for lithium-ion batteries, Electrochim. Acta 53 (22) (2008) 6497–6503.
[53] P. Chen, F. Yang, A. Kostka, W. Xia, Interaction of cobalt nanoparticles with oxygen- and nitrogen-functionalized carbon nanotubes and impact on nitrobenzene hydrogenation catalysis, ACS Catal. 4 (5) (2014) 1478–1486.
[54] H. Xiong, M.A. Motchelaho, M. Moyo, L.L. Jewell, N.J. Coville, Correlating the preparation and performance of cobalt catalysts supported on carbon nanotubes and carbon spheres in the Fischer–Tropsch synthesis, J. Catal. 278 (1) (2011) 26–40.
[55] V. Ţucureanu, A. Matei, A.M. Avram, FTIR spectroscopy for carbon family study, Critical Rev. Anal. Chem. 46 (6) (2016) 502–520.
[56] Y. Xie, F. Dong, S. Heinbuch, J.J. Rocca, E.R. Bernstein, Oxidation reactions on neutral cobalt oxide clusters: experimental and theoretical studies, Phys. Chem. Chem. Phys. 12 (4) (2010) 947–959.
[57] R. Baker, P. Harris, R. Thomas, R. Waite, Formation of filamentous carbon from iron, cobalt and chromium catalyzed decomposition of acetylene, J. Catal. 30 (1) (1973) 86–95.
[58] B. Liu, K. Zhou, Recent progress on graphene-analogous 2D nanomaterials: properties, modeling and applications, Progress Mater. Sci. (2018).
[59] L. Qu, Y. Liu, J.-B. Baek, L. Dai, Nitrogen-doped graphene as efficient metal-free electrocatalyst for oxygen reduction in fuel cells, ACS Nano 4 (3) (2010) 1321–1326.
[60] S. Jiang, C. Zhu, S. Dong, Cobalt and nitrogen-cofunctionalized graphene as a durable non-precious metal catalyst with enhanced ORR activity, J. Mater. Chem. A 1 (11) (2013) 3593–3599.
[61] R.I. Jafri, N. Rajalakshmi, S. Ramaprabhu, Nitrogen doped graphene nanoplatelets as catalyst support for oxygen reduction reaction in proton exchange membrane fuel cell, J. Mat. Chem. 20 (34) (2010) 7114–7117.
[62] D.W. Wang, F. Li, M. Liu, G.Q. Lu, H.M. Cheng, 3D aperiodic hierarchical porous graphitic carbon material for high-rate electrochemical capacitive energy storage, Angew. Chem. Int. Ed. 120 (2) (2008) 379–382.
[63] M. Liu, L. Gan, W. Xiong, F. Zhao, X. Fan, D. Zhu, Z. Xu, Z. Hao, L. Chen, Nickel-doped activated mesoporous carbon microspheres with partially graphitic structure for supercapacitors, Energy Fuels 27 (2) (2013) 1168–1173.
[64] R. Liu, D. Wu, X. Feng, K. Müllen, Nitrogen-doped ordered mesoporous graphitic arrays with high electrocatalytic activity for oxygen reduction, Angew. Chem. Int. Ed. 122 (14) (2010) 2619–2623.
[65] J.M.R. Gallo, G. Gatti, A. Graizzaro, L. Marchese, H.O. Pastore, Novel mesoporous carbon ceramics composites as electrodes for direct methanol fuel cell, J. Power Sources 196 (20) (2011) 8188–8196.
[66] R. Miao, Z. Luo, W. Zhong, S.Y. Chen, T. Jiang, B. Dutta, Y. Nasr, Y. Zhang, S.L. Suib, Mesoporous TiO_2 modified with carbon quantum dots as a high-performance visible light photocatalyst, Appl. Catal. B-Environ. 189 (2016) 26–38.
[67] L.L. Perreault, S. Giret, M. Gagnon, J. Florek, D. Lariviere, F. Kleitz, Functionalization of mesoporous carbon materials for selective separation of lanthanides under acidic conditions, ACS Appl. Mater. Interfaces 9 (13) (2017) 12003–12012.
[68] W.K. Oh, H. Yoon, J. Jang, Size control of magnetic carbon nanoparticles for drug delivery, Biomaterials 31 (6) (2010) 1342–1348.
[69] F. Ma, H. Zhao, L. Sun, Q. Li, L. Huo, T. Xia, S. Gao, G. Pang, Z. Shi, S. Feng, - A facile route for nitrogen-doped hollow graphitic carbon spheres with superior performance in supercapacitors, J. Matr. Chem. 22 (27) (2012) 13464–13468.
[70] L.F. Chen, X.D. Zhang, H.W. Liang, M. Kong, Q.F. Guan, P. Chen, Z.Y. Wu, S.H. Yu, Synthesis of nitrogen-doped porous carbon nanofibers as an efficient electrode material for supercapacitors, ACS Nano 6 (8) (2012) 7092–7102.